Fiber inline interferometric refractive index sensors fabricated by femtosecond laser and fusion splicing

Yingyu Yu (于鹰宇), Lan Jiang (姜 澜), Benye Li (李本业), Zhitao Cao (曹志涛), and Sumei Wang (王素梅)*

Nanomanufacturing Fundamental Research Joint Laboratory of National Science Foundation of China, School of Mechanical Engineering, Beijing Institute of Technology, Beijing 100081, China

**Corresponding author: wangsumei@bit.edu.cn*

Received July 4, 2013; accepted September 25, 2013; posted online November 4, 2013

A fiber inline interferometric refractive index (RI) sensor consisting of a microchannel and a fiber taper is proposed in this letter. The microchannel is fabricated by combining femtosecond laser micromachining and arc fusion splicing. No subsequent chemical etching process is needed. Three sensors with microchannel widths of 4, 8, and 10 μm are prepared. The sensitivity in the RI range from 1.33 to 1.35 is up to ~361.29 nm/RIU at the microchannel width of 8 μm. The sensitivity is ~20 times greater than that of the paired taper-based MZI sensors and long period fiber grating pair MZI sensors.

OCIS codes: 060.2280, 060.2370, 220.4610.
doi: 10.3788/COL201311.110603.

A number of optical fiber sensors have been proposed for refractive index (RI) measurements, such as long period fiber gratings (LPFGs)[1], fiber Bragg gratings (FBGs)[2], interferometers[3], resonant devices[4−6], and other configurations[7]. These devices show promising applications in chemical and biological sensing. However, the FBG sensors in Ref. [2] need complex fabrication processes. Micro resonator-based RI sensors have low reliability. Thus, Tian *et al*. proposed compact tapered-fiber-based interferometric sensors for RI measurements[8,9]. The interferometric RI sensors offer a low-cost and simple fabrication process[8,9], but their sensitivity is relatively low (~20 nm/RIU in the RI range from 1.33 to 1.36).

Recent developments in femtosecond (fs) laser technology have opened new possibilities for the fabrication of micro/nanoscale three-dimensional structures in various solid materials with greatly reduced collateral damage[10]. New opportunities for laser micromachining of fiber optic devices are possible using ultrashort laser pulses. Various structures have been fabricated in fibers using fs lasers, such as microchannels[11,12], microholes[13], Fabry–Perot interferometers[14−16], and Mach–Zehnder interferometers (MZIs)[17−19]. In terms of microchannels, Lai *et al*. proposed an effective method for fabricating microchannels in conventional single-mode fibers, and these microchannels have been successfully used in RI measurements[11,20−22]. However, the microchannel is realized by selective chemical etching with a hydrofluoric acid solution to remove the laser-modified material within the fiber. Moreover, a special setup is needed to alleviate the beam defocusing distortions caused by the curved surface of the fiber.

In this letter, we propose a MZI consisting of a fs laser-fabricated microchannel and a fiber taper prepared by fusion splicing. The microchannel is embedded into the fiber through direct fs laser pulse ablation and arc fusion splicing technique, without subsequent chemical etching process. Microchannels with three different widths of 4, 8, and 10 μm have been fabricated. In such a MZI sensor, the guided light wave directly interacts with the measured fluid; thus, high sensitivity can be achieved. The obtained maximum sensitivity in the RI range from 1.333 to 1.335 is 361.29 nm/RIU when the microchannel width is 8 μm. The sensitivity is ~20 times greater than that of the taper-based[9] or LPFG pair-based MZI sensors[3].

The schematic of the MZI consisting of a fiber taper and a microchannel separated by a certain distance L is shown in Fig. 1(a). In our experiments, a fs laser (Spectra–Physics) with a pulse width of 35 fs is used to fabricate the microchannel on the cleaved fiber end. The center wavelength and repetition rate of the laser are 800 nm and 1 kHz, respectively. A combination of a half-wave plate and a polarizer is used to reduce the laser power, and then several neutral density filters are used to further reduce the laser power to the desired values. The laser beam is focused on the fiber core by a 20× microscopic objective (N.A. = 0.45, Olympus), and the beam diameter at the focal plan is approximately 1 to 2 μm. The single pulse energy before the objective lens is around 0.5 μJ. The optical fiber is an enhanced telecom fiber SMF-28e (Corning, Inc.) with a core diameter of 8.2 μm, a cladding diameter of 125 μm, and a numerical aperture of 0.14. During the fabrication process, the cleaved fiber end is mounted on a six-axial moving stage with a resolution of 1 μm in the x and y directions and 0.5 μm in the z direction. A rectangular scanning program is launched with a scanning speed of 100 μm/s, and the stage decreases by 0.5 μm after each layer is ablated. The cross-section of the microchannel is rectangular after fabrication. The surface roughness of the channel affects the whole loss of the sensor, but not the sensitivity. The microchannel is first fabricated in the cleaved fiber end by the focused fs laser beam. A normal fiber end is then spliced to the fs laser-processed

fiber with appropriate arc conditions. The centerline of the microchannel is aligned to coincide with the fiber end. Microchannels with three different widths of 4, 8, and 10 μm are fabricated in the fiber end. All the channels have a depth of 10 μm. One of the microchannels with a width of 10 μm is shown in Fig. 1(c).

An abrupt tapered fiber is fabricated through fusion-splicing, 10 mm away from the microchannel. Details on the fabrication of the fiber taper can be found elsewhere[23]. The microscope image of the fiber taper with a length and a diameter of ~100 μm is shown in Fig. 1(b). The three interferometers with widths of 4, 8, and 10 μm are denoted as MZI-1, MZI-2, and MZI-3, respectively.

To measure the transmission spectra, one end of the interferometer is connected to a tunable laser (Agilent 81980A) with a wavelength range from 1 465 to 1 575 nm, whereas the other end is connected to an optical power meter (Agilent 8163B). The transmission spectra of the three interferometers with different microchannel widths of 4, 8, and 10 μm are illustrated in Fig. 2. The transmission losses of the fibers with only one microchannel are 4.5, 9, and 12 dB when the microchannel widths are 4, 8, and 10 μm, respectively (Fig. 2). When a fiber taper is added by fusion splicing, interference fringes are observed on the spectra. The extinction ratios are

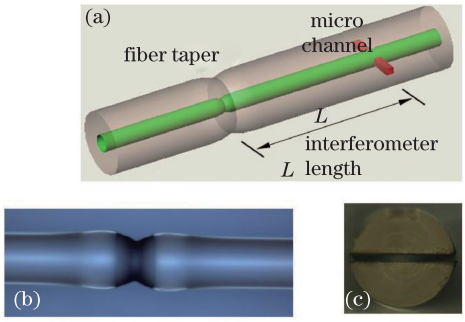

Fig. 1. Proposed MZI sensor consisting of a fiber taper and a microchannel. (a) Schematic diagram and (b) microscope images of the fiber taper with diameter and length of ~100 μm; (c) microchannel with a width of ~10 μm.

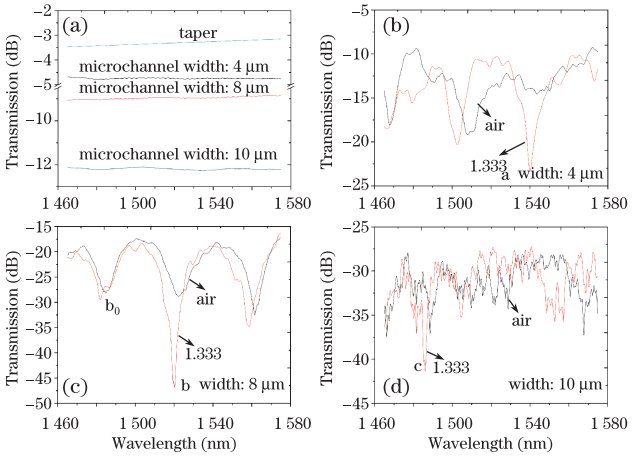

Fig. 2. Transmission spectra of the MZIs in air and in the liquid with RI = 1.333. (a) A single taper and single microchannel with different widths in air: (b) 4, (c) 8, and (d) 10 μm, respectively.

approximately 8, 10, and 6 dB for MZI-1, MZI-2, and MZI-3, respectively. When the microchannel width is larger than the diameter of the fiber core, more light will be reflected and scattered by the cross section when passing through the microchannel, producing obvious loss and noise. Therefore, the sensor with a microchannel width of 10 μm has larger noise and loss than the others.

The fiber taper is used to couple part of the fundamental core mode to higher cladding modes. At the same time, some energy left in the core continues to propagate forward in the fiber core. Parts of the cladding modes are coupled back to the core when meeting the microchannel, which is apart from the taper with a distance of 10 mm. The phase difference between the cladding mode $LP_{\rm nm}$ and core mode LP_{01} traveling the same distance L can be expressed as $\varphi{=}2\pi\Delta n_{\rm eff}\ L/\lambda$, where $\Delta n_{\rm eff}$ is the difference of the effective refractive indices between the core and cladding modes, and λ is the operating wavelength. The interference signal reaches its minimum when $2\pi\Delta n_{\rm eff}\ L/\lambda{=}(2k{+}1)\ \pi$, where k is an integer. The effective refractive index of the cladding mode changes with the variations in the external refractive index, resulting in a shift in the maximum attenuation wavelength. The sensitivity can be expressed as[24]

$$\frac{{\rm d}\lambda_{\rm v}}{{\rm d}n_{\rm ext}} = -\frac{2L}{2k+1}\frac{\partial n_{\rm cl,m}^{\rm eff}}{\partial n_{\rm ext}}\Bigg/\left[1-\frac{2L}{2k+1}\left(\frac{\partial n_{\rm core}^{\rm eff}}{\partial\lambda}-\frac{\partial n_{\rm cl,m}^{\rm eff}}{\partial\lambda}\right)\right], \quad (1)$$

where $n_{\rm ext}$ is the external refractive index; k is an integer, λ_ν is the maximum attenuation wavelength of the $k_{\rm th}$ order, and $n_{\rm core}^{\rm eff}$ and $n_{\rm cl,m}^{\rm eff}$ are the effective RIs of the core and the $m_{\rm th}$ order cladding modes, respectively. The RI of the channel directly affects the light transmission behavior in the core-cladding interface[13]. The change in the channel fluids can directly influence the interference spectra of the interferometers, which leads to change in the maximum attenuation wavelength. As shown in Fig. (2), the extinction ratios become larger when the MZIs are immersed into water. Especially for MZI-2, the extinction ratio is 25 dB, mainly because an optimal interference condition is obtained in the water caused by the reduction in the RI difference.

The RIs of the proposed fiber sensors are measured in a clean room with almost constant temperature to eliminate the effects caused by temperature fluctuations. During the measurements, all sensors are straightened and fixed on a fiber holder to avoid bending-induced signal change. Salt solutions with different concentrations (0.0%, 0.99%, 1.96%, 2.91%, 3.85%, 4.76%, 5.66%, and 6.54% (mass percent)) are used in the experiments. The corresponding RIs are 1.3330, 1.3348, 1.3366, 1.3383, 1.3400, 1.3418, 1.3435, and 1.3453, respectively[25]. The sensor is cleaned by distilled water and dried air between each measurement.

The maximum attenuation peak wavelengths in 1.3330 are chosen as the starting recorded wavelength, which are marked by a, b, and c in Fig. 2. These wavelengths denote the maximum attenuation wavelengths of 1539.96, 1520.26, and 1486.01 nm, respectively. The wavelength

shifts of the three maximum attenuation peaks with respect to the change in external RI are shown in Fig. 3. All attenuation peaks shift to longer wavelengths with the increasing RI, with corresponding sensitivities of 268.46, 361.29, and 228.98 nm/RIU. The RI sensitivity of MZI-2 is higher than the others because the difference in the effective index between the core mode filled with liquid to be measured and the cladding mode is largest when the microchannel width is closest to the diameter of the fiber core (8.2 μm). In the same RI range, the sensitivity is ~20 times greater than those of the LPFG pair MZI sensors[3] and the tapered-fiber pair MZI sensors[9]. Although the sensitivity is lower than that reported in Refs. [17,18], the fabrication time is much shorter, and the structure is more robust.

We also compare the sensitivities between two attenuation peaks. For MZI-2, two attenuation peaks, marked by b_0 and b in Fig. 2, are chosen as the recorded wavelengths. The results show that the sensitivity of the attenuation peak b_0 is 236.59 nm/RIU (Fig. 4). The change in the measured transmission spectra with the RI is also displayed in Fig. 4, which demonstrates that the RI sensitivity varies with the maximum attenuation peaks. These changes are primarily due to the fact that different cladding modes have different mode field areas, and the sensitivities are different for various cladding modes. Li *et al.*[26] recently reported that higher-order cladding modes have larger mode field areas and are more easily affected by the surrounding RI. Thus, higher-order cladding modes exhibit lower mode indices and higher sensitivities. The different sensitivity results shown in our study are in accordance with the peak shift discrepancy reported in Ref. [26].

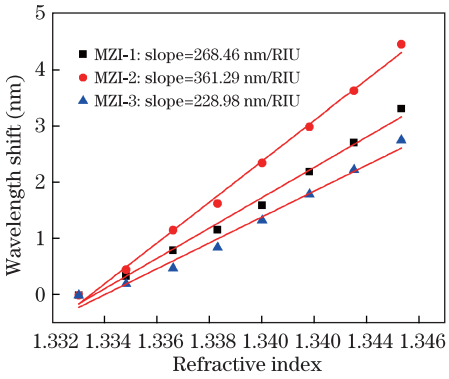

Fig. 3. Wavelength shifts of the maximum attenuation peaks of the three MZIs caused by the change in RI.

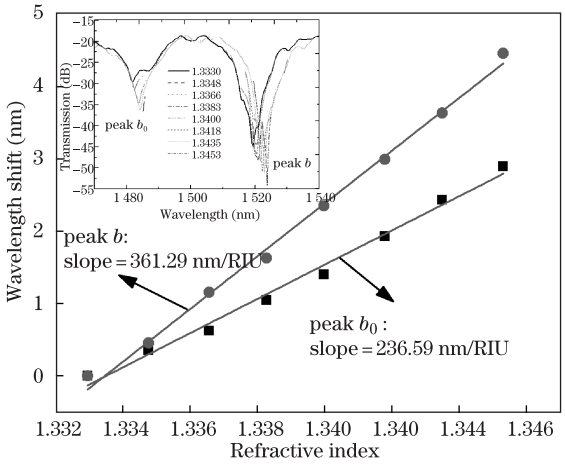

Fig. 4. Wavelength shifts of two different attenuation peaks of MZI-2 caused by change in external RI. The inset shows the changes in the measured spectra.

In conclusion, we propose a novel RI sensor based on a fs laser-fabricated microchannel combined with a fusion-spliced fiber taper. The microchannel is obtained by combining direct fs laser pulse ablation and the arc fusion-splicing technique, without subsequent chemical etching process. Three types of interferometers are fabricated with different microchannel widths of 4, 8, and 10 μm. The results demonstrate that the RI sensitivity depends on the microchannel width and the selection of the attenuation peaks. The obtained maximum sensitivity in the RI range from 1.33 to 1.35 is 361.29 nm/RIU when the microchannel width is 8 μm. The sensitivity is ~20 times greater than that of the paired taper-based or LPFG pair MZI sensors. Moreover, the proposed MZI has high potential for developing microfluidic fiber devices for chemical and biological sensing applications.

This work was supported by the National "973" Program of China (No. 2011CB013000) and the National Natural Science Foundation of China (Nos. 90923039 and 51105038).

References

1. S. W. James and R. P. Tatam, Meas Sci Technol. **14,** R49 (2003).
2. A. Iadicicco, A. Cusano, A. Cutolo, R. Bernini, and M. Giordano, IEEE Photon. Technol. Lett. **16,** 1149 (2004).
3. T. Allsop, R. Reeves, D. J. Webb, I. Bennion, and R. Neal, Rev. Sci. Instrum. **73,** 1702 (2002).
4. N. M. Hanumegowda, C. J. Stica, B. C. Patel, I. M.White, and X. Fan, Appl. Phys. Lett. **87,** 201107 (2005).
5. I. M. White and X. Fan, Opt. Express **16,** 1020 (2008).
6. N. Lin, L. Jiang, S. Wang, L. Yuan, H. Xiao, Y. Lu, and H. L. Tsai, Appl. Opt. **49,** 6463 (2010).
7. X. Guo and L. Tong, Opt. Express **16,** 14429 (2008).
8. Z. B. Tian, S. S-H. Yam, and H. P. Loock, Opt. Lett. **33,** 1105 (2008).
9. Z. B. Tian, S. S-H. Yam, J. Barnes, W. Bock, P. Greig, J. M. Fraser, H. P. Loock, and R. D. Oleschuk, IEEE Photon Technol. Lett. **20,** 626 (2008).
10. L. Jiang and H. L. Tsai, J. Appl. Phy. **100,** 023116 (2006).
11. Y. Lai, K. Zhou, L. Zhang, and I. Bennion, Opt. Lett. **31,** 2559 (2006).
12. A. V. Brakel, C. Grivas, M. N. Petrovich, and D. J. Richardson, Opt. Express **15,** 8731 (2007).
13. Y. Wang, D. N. Wang, M. Yang, W. Hong, and P. Lu, Opt. Lett. **34,** 3328 (2009).
14. Y. J. Rao, M. Deng, D. W. Duan, X. C. Yang, T. Zhu, and G. H. Cheng, Opt. Express **15,** 14123 (2007).
15. T. Wei, Y. K. Han, Y. J. Li, H. L. Tsai, and H. Xiao, Opt. Express **16,** 5764 (2008).
16. C. H. Lin, L. Jiang, H. Xiao, Y. H. Chai, S. J. Chen, and H. L. Tsai, Opt. Lett. **34,** 2408 (2009).
17. Y. Wang, M. Yang, D. N. Wang, S. Liu, and P. Lu, J. Opt. Soc. Am. B **27,** 370 (2010).
18. L. Jiang, L. J. Zhao, S. M. Wang, J. P. Yang, and H. Xiao, Opt. Express **19,** 17591 (2011).

19. M. Park, S. Lee, W. Ha, D. K. Kim, W. Shin, I. B. Sohn, and K. Oh, IEEE Photon Technol. Lett. **21,** 1027 (2009).
20. K. Zhou, Y. Lai, X. Chen, K. Sugden, L. Zhang, and I. Bennion, Opt. Express **15,** 15848 (2007).
21. H. Fu, K. Zhou, P. Saffari, C. Mou, L. Zhang, S. He, and I. Bennion, IEEE Photon. Technol. Lett. **20,** 1609 (2008).
22. K. Zhou, Z. Yan, L. Zhang, and I. Bennion, Opt. Express **19,** 11769 (2011).
23. Y. Yu, L. Jiang, B. Li, S. Wang, and H. Wu, Chin. Opt. Lett. **10,** 122801 (2012).
24. B. Li, L. Jiang, S. Wang, L. Y. Zhou, H. Xiao, and H. L. Tsai, Sensors **11,** 5729 (2011).
25. Relationship between Salt Solution and Sugar Concentration (Brix) and refractive index at 20 °C. Available online: http://www.topac.com/salinity_brix.html (accessed on 12 August 2011).
26. Y. Li, E. Harris, L. Chen, and X. Bao, Opt. Express **18,** 8135 (2010).